ISBN: 978-3-95450-211-0 doi:10.18429/JACoW-SRF2019-THP102

UNCERTAINTY QUANTIFICATION OF A QUADRUPOLE-RESONATOR FOR RADIO FREQUENCY CHARACTERIZATION OF SUPERCONDUCTORS *

P. Putek†1, S. Gorgi Zadeh[1], University of Rostock, [D-18059] Rostock, Germany
M. Wenskat[2,3], W. Hillert[2,3], University of Hamburg, [D-22607] Hamburg, Germany
[3]German Electron Synchrotron, [D-22607] Hamburg, Germany
U. van Rienen[1,4], University of Rostock, [D-18059] Rostock, Germany
[4] Department Life, Light & Matter, [D-18051] Rostock, Germany

Abstract

To explore the fundamental properties of superconducting materials used in modern particle accelerators, high precision surface-resistance measurements in a dedicated testing equipment are of key importance. The quadrupole resonator, originally developed at CERN, and then successfully modified at the Helmholtz-Zentrum Berlin, is ideally suited for characterization of samples at temperatures of 1.8 K to more than 20 K, RF fields of up to 120 mT and frequencies of 433 MHz, 866 MHz and 1.3 GHz. In the past years, this set-up has been subject of intensive research on both its capabilities and limitations. Yet, one of the main challenges is the accuracy of the surface resistance measurement, which is determined by both the uncertainty in the RF measurement and manufacturing imperfections related to the production tolerances such as quenching and chemical polishing processes, etc. In this contribution, we focus on the influence of key geometrical parameters on three operating modes of the quadrupole resonator especially on the third mode since the surface-resistance measurements show some unexpected behavior for this frequency.

INTRODUCTION

In modern particle accelerators, superconducting radio frequency (SRF) cavities are applied to provide large accelerating gradients to high current beams while demanding moderate power requirements. Since power consumption and maximum accelerating gradient are mainly determined by the material properties, the surface resistance and the critical RF-field, the physical features of those materials used for building cavities are of key importance. Particularly, systematic research on superconductors requires conducting precision measurements of the RF properties as a function of an applied magnetic field, the operating temperature and the frequency, respectively.

The quadrupole resonator (QPR), originally developed at CERN [1], and then successfully modified at the Helmholtz-Zentrum Berlin, is dedicated for the characterization of samples at temperatures of 1.8 K to more than 20 K, RF fields of up to 120 mT and frequencies of 433 MHz, 866 MHz and 1.3 GHz [2, 3]. This device is treated as a case study in our research. Its cross sectional view is schematically shown in Fig. 1. The structure consists of a pillbox-like niobium cavity with four vertical niobium rods, collinearly arranged inside the resonator. The rods are welded to the top-plate of the cavity. At their lower end, they are bent into semi-annular pole shoes and positioned a short distance over the sample surface. Furthermore, at the bottom of the cylinder, the calorimetry chamber is mounted as inner conductor of a coaxial structure, which is additionally thermally decoupled from the resonator. It is equipped with a resistive DC heater and sensors placed on the bottom of the disc-shaped sample. This design provides focusing of the RF magnetic field into the area of the sample. The resulting power dissipation can then be measured by temperature probes inside the calorimetry chamber. As a result, the surface resistance R_S is studied by means of the so-called "RF-DC-compensation" method proposed in [1].

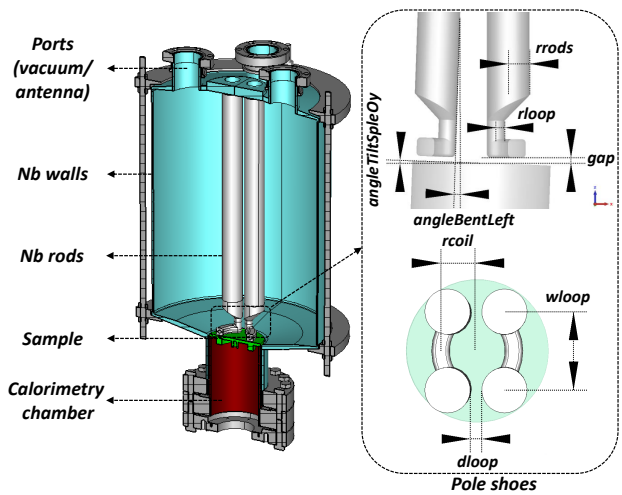

Figure 1: Schematic view of the Quadrupole Resonator (left) and a parameterized model of the pole shoes (right).

Measurement Principle and Uncertainties

To measure the surface resistance of a sample, the QPR utilizes the "RF-DC-compensation" method mentioned above. First, the sample is heated to a desired temperature of interest T_{int} using the DC heater, which operates in a feedback loop with a proportional–integral–derivative (PID) controller. This allows for determining the heater power P_{DC1}

* Work supported by the German Federal Ministry for Research and Education BMBF under contract 05H18HRRB1.
† piotr.putek@uni-rostock.de

ISBN: 978-3-95450-211-0 doi:10.18429/JACoW-SRF2019-THP102

required for temperature stabilization. Next, the RF is turned on, which results in increasing the heat load on the sample. Then, the temperature controller reduces the power in order to reach the thermal equilibrium for the initial temperature T_{int}. In steady state, the reduced heater power P_{DC2} is determined and recorded. Hence, the RF dissipated power on the sample surface Ω_{S} is defined by the difference in the DC heater power and it is given by

$$P_{\text{RF}}(\boldsymbol{p}) = [P_{\text{DC1}}(\cdot) - P_{\text{DC2}}(\cdot)] = \frac{1}{2}\int_{\Omega_{\text{S}}} R_{\text{S}}(\boldsymbol{p})\,|\vec{H}(\boldsymbol{p})|^2 d\boldsymbol{x} \tag{1}$$

with the magnetic field $\vec{H}$ and certain model parameters $\boldsymbol{p}$.

Moreover, assuming that the surface resistance R_{S} is independent of $\vec{H}$ and homogeneously distributed across Ω_{S}, it can be pulled outside of the integral in (1) and then be approximated by

$$R_{\text{S}}(\boldsymbol{p}) \approx \frac{2\,[P_{\text{DC1}}(\boldsymbol{p}) - P_{\text{DC2}}(\boldsymbol{p})]}{\int_{\Omega_{\text{S}}} |\vec{H}(\boldsymbol{p})|^2 d\boldsymbol{x}}, \tag{2}$$

where the integral term appearing in the denominator is not experimentally accessible. But it can be numerically computed as a product of a simulation constant c and the stored energy U in the cavity. The latter quantity is measured using a pickup antenna. For details, we refer to [4]. Consequently, the varied sources of uncertainties are associated with the above described measurement methodology.

Summarising, the accuracy of the surface resistance measurement is mainly determined by the uncertainty in

- the RF measurement methodology such as cable calibration errors, power meter tolerances,
- manufacturing imperfections, which affect both material and geometrical parameters,
- modelling issues such as error propagation, number representation, model calibration using measurement quantities, etc.

The associated uncertainties have impact not only on the measurement methodology, but also on the stability and operational conditions of the QPR.

Thus, we investigate the uncertainty propagation in the three-dimensional (3D) model of the QPR. Special focus is put on the influence of the geometrical parameters on reliable operation of the QPR under working conditions.

PROBLEM FORMULATION

To study the impact of geometrical parameters on the functioning of the QPR in terms of objective functions, we consider a hyperbolic partial differential equation (PDE) with random input parameters. Thereby, the input variations, which reflect the manufacturing imperfections arisen from the industrial processes are modeled by the Polynomial Chaos expansion (PCE) technique. The resulting stochastic model is solved using the stochastic collocation method [5, 6].

Stochastic Forward Problem

The mathematical model of the QPR can be described in terms of a hyperbolic boundary value problem on the spatial domain D, which is schematically shown in Fig. 1. More precisely, it is defined by the Helmholtz equation [2]

$$\nabla \times \nabla \times \vec{H}(\theta) - \omega^2(\theta)\,\mu(\theta)\,\epsilon(\theta)\vec{H}(\theta) = 0, \tag{3a}$$

$$\boldsymbol{n} \cdot \vec{H}(\theta) = 0, \tag{3b}$$

endowed with the so-called perfect boundary condition. Here, θ is defined as $\theta := (\boldsymbol{r}, f, \boldsymbol{p}) \in D \times \mathcal{F} \times \Pi$ where D, $\mathcal{F}$ and Π refer to a computational domain in $\mathbb{R}^3$, $f \in \mathcal{F}$ in some frequency range $\mathcal{F} \subseteq \mathbb{R}$ and Π a multidimensional parameter domain, respectively. Moreover, assuming that the corresponding model is characterized by linear and isotropic (deterministic) materials, σ and μ denote the electric conductivity and the magnetic permeability. The complex electric permittivity is expressed by $\underline{\epsilon} := \epsilon + \frac{\sigma}{\mathrm{j}\omega}$ with the real permittivity ϵ and $\mathrm{j} = \sqrt{-1}$.

Parametrization of Random Inputs

In the stochastic model (3a)–(3b), we assume that certain input parameters suffer from uncertainty due to manufacturing imperfections, see, e.g., [7, 8]. First, we introduce $\xi_1 \ldots, \xi_Q$, $(Q = 10)$ normally distributed random variables to represent 10 variations of geometric parameters. Then, due to the infinite support of the normal density function and manufacturing constraints these ξ_i are transformed to a bounded domain as follows

$$p_i(\xi_i) := \delta_i \cdot \Upsilon(\xi_i), \quad \text{for } i = 1, \ldots, Q, \quad \Upsilon(\cdot) := \arctan(\cdot),$$

where δ_i denotes fixed perturbation magnitudes. This yields the definition of a random vector $\boldsymbol{p} = \boldsymbol{p}(\boldsymbol{\xi}) \in \mathbb{R}^Q$ with image space $\Gamma \in \mathbb{R}^Q$ and with corresponding probability density function (PDF) $\boldsymbol{\rho}$. As a result, the numerical computation can be conducted in $(\Gamma, \mathcal{B}^Q, \rho \mathrm{d}\boldsymbol{p})$ with the 10-dimensional Borel space $\mathcal{B}^{10}$ and a probability measure $\rho \mathrm{d}\boldsymbol{p}$.

In the end, given an integrable function f, the corresponding expected value is defined as

$$\mathbb{E}[f(\boldsymbol{p}(\boldsymbol{\xi}))] := \int_{\Gamma} f(\mathbf{p})\,\rho(\boldsymbol{p})\,\mathrm{d}\boldsymbol{p},$$

which induces an inner product of two square integrable functions f and g

$$\langle f(\boldsymbol{p}), g(\boldsymbol{p})\rangle_\rho := \mathbb{E}\,(f(\boldsymbol{p})g(\boldsymbol{p}))$$

and a corresponding L^2_ρ norm $\langle\cdot,\cdot\rangle_\rho$ [9]. Likewise, the variance of $f(\boldsymbol{p})$ is given by

$$\mathrm{Var}[f(\boldsymbol{p})] = \mathbb{E}[f(\boldsymbol{p})^2] - \mathbb{E}[f(\boldsymbol{p})]^2. \tag{4}$$

Pseudo-spectral Approach

Now, for the uncertainty quantification of (3a)–(3b), first we introduce the truncated PCE [9] for $f \in L^2_\rho$ in the following form

$$\widetilde{f}(\boldsymbol{p}) \approx \sum_{m=0}^{M} f_m\,\Phi_m(\boldsymbol{p}), \tag{5}$$

ISBN: 978-3-95450-211-0 doi:10.18429/JACoW-SRF2019-THP102

where f_m are *a priori* unknown coefficient functions to be determined by means of the pseudo-spectral approach and $\Phi_m : \mathbb{R}^Q \to \mathbb{R}$ denote a respective basis of multivariate polynomials, which correspond to the distribution of random input parameters. For instance, the application of the uniform distribution implies the Legendre polynomials, while the Hermite polynomials correspond to Gaussian-type PDF, respectively.

In our work, for the calculation of f_m in equation (5) the pseudo-spectral approach is used [5]. According to this method, the provided solutions at quadrature points is projected on the basis polynomials using

$$f_m = \left\langle \widetilde{f}(\boldsymbol{p}), \Phi_m(\boldsymbol{p}) \right\rangle_\rho . \tag{6}$$

In particular, to approximate the probabilistic integrals of (6), the Stroud formulas with a constant weight function [5] are applied. This yields the multi-dimensional quadrature rule with associated weights w_k and points $\boldsymbol{p}^k$ $(k = 1, \ldots, K)$ in the following form

$$f_m \approx \sum_{k=1}^{K} w_k \, \widetilde{f}\left(\boldsymbol{p}^{(k)}\right) \, \Phi_m\left(\boldsymbol{p}^{(k)}\right). \tag{7}$$

This type of quadrature methods is exact for multivariate polynomials up to the degree d_{PC}. For $d_{\mathrm{PC}} = 3$ it needs $K = 2Q = 20$, while for $d_{\mathrm{PC}} = 5$, it requires $K = 2Q^2 + 1 = 201$ deterministic runs of a respective model. This approach is highly efficient in particular for large numbers of parameters [9] but their accuracy is fixed and cannot be improved. Finally, when using quadrature rules, the expected value and the variance are approximated by

$$\mathbb{E}\left[\widetilde{f}(\boldsymbol{p})\right] \approx f_0, \quad \mathrm{Var}\left[\widetilde{f}(\boldsymbol{p})\right] \approx \sum_{m=1}^{M} |f_m|^2, \tag{8}$$

using $\Phi_0 = 1$ [5]. Based on (5), also other quantities such as the local sensitivity and the variance-based global sensitivity can easily be calculated [10].

Variance-based and Local Sensitivity Analysis

The Sobol decomposition yields the normalized variance-based sensitivity coefficients in the form [10, 11]

$$S_j = \frac{\mathrm{V}_j}{\mathrm{Var}(f)} \quad \text{with} \quad \mathrm{V}_j := \sum_{i \in \mathbb{I}_j} |f_i|^2 \, j = 1, \ldots, Q, \tag{9}$$

with sets $\mathbb{I}_j := \{j \in \mathbb{N} : \Phi_j(\boldsymbol{p})$ is not constant in $p_j\}$ and $\mathrm{Var}(f)$ denotes the total variance. Note that $0 \le S_j \le 1$, where a value close to 1 means a large contribution to the variance and vice versa.

Furthermore, differentiating (5) with respect to p_j allows for determining $\partial \tilde{f}/\partial p_j$ at any value of $\boldsymbol{p}$ defined as

$$\left.\frac{\partial \tilde{f}}{\partial p_j}\right|_{p_j = \overline{p}_j} = \sum_{i=0}^{N} f_i \frac{\partial \Phi_i}{\partial p_j} \frac{\partial \boldsymbol{p}}{\partial \xi_j}, \quad j = 1, \ldots, Q. \tag{10}$$

The p_j-th mean sensitivity is obtained by integrating over the whole parameter space [9].

NUMERICAL RESULT AND DISCUSSION

In our study, to assess the influence of the particular random parameters within the design of the QPR, the following stochastic objective functions are considered

- operating frequencies to elaborate their deviation :

$$\begin{aligned} f_{1,1}(\boldsymbol{p}) &= 0.429[\mathrm{GHz}], \\ f_{1,2}(\boldsymbol{p}) &= 0.866[\mathrm{GHz}], \\ f_{1,3}(\boldsymbol{p}) &= 1.311[\mathrm{GHz}], \end{aligned} \tag{11a}$$

- the focusing factor to investigate the focus of the magnetic fields onto the sample:

$$f_{2,k}(\boldsymbol{p}) = \frac{1}{2U} \int_{\Omega_{\mathrm{S}}} \left|\vec{H}(\boldsymbol{p})\right|^2 \mathrm{d}\boldsymbol{x}, \tag{11b}$$

- the homogeneity factor to measure the homogeneity of the magnetic field on the sample :

$$f_{3,k}(\boldsymbol{p}) = \langle H^2(\boldsymbol{p}) \rangle_{\Omega_{\mathrm{S}}} / \hat{H}^2_{\Omega_{\mathrm{S}}}(\boldsymbol{p}), \tag{11c}$$

- the operating range to increase the maximum attainable field on the sample:

$$f_{4,k}(\boldsymbol{p}) = \hat{H}_{\Omega_{\mathrm{S}}}(\boldsymbol{p}) / \hat{H}_{\Omega_{\mathrm{R}}}(\boldsymbol{p}), \tag{11d}$$

- the risk of field emission to investigate the limitation caused by high electric fields:

$$f_{5,k}(\boldsymbol{p}) = \hat{H}_{\Omega_{\mathrm{S}}}(\boldsymbol{p}) / \hat{E}_{\Omega_{\mathrm{R}}}(\boldsymbol{p}), \tag{11e}$$

- the dimensionless factor to study measurement bias by calculating the ratio of the losses on the sample to the surface integral of the square of the magnetic field that penetrates into the coaxial gap around the calorimetry chamber:

$$f_{6,k}(\boldsymbol{p}) = \frac{\int_{\Omega_{\mathrm{S}}} \left|\vec{H}(\boldsymbol{p})\right|^2 \mathrm{d}\boldsymbol{x}}{\int_{\Omega_{\mathrm{F}}} \left|\vec{H}(\boldsymbol{p})\right|^2 \mathrm{d}\boldsymbol{x}} \tag{11f}$$

with the subscript $k = 1, 2, 3$ used for particular operating frequencies. $\hat{H} = |\hat{\vec{H}}|$, $\hat{E} = |\hat{\vec{E}}|$ and $\langle \cdot \rangle$ denote the peak magnetic field and the peak electric field calculated either on the surface of the sample Ω_{S} or on the surface of the rods Ω_{R}, and the average operator, respectively. Ω_{F} refers to the region of the flange (calculated at the coaxial gap, 70 mm below the surface of the sample) and U is the stored energy in the QPR. A detailed description of the parameters is given in [2].

For the uncertainty quantification, we assume that certain geometrical parameters suffer from uncertainty due to manufacture imperfections, see, e.g., , [7, 8]. These input variations are modeled using Hermite polynomials of order $d_{\mathrm{PC}} = 3$. More specifically, in our work we consider Q = 10 normally distributed geometrical variables, which detailed description is summarized in the Table 1. For all uncertain geometrical parameters, the lower δ_{L_j} and upper bounds δ_{U_j} are specified by $\overline{x}_j \mp 3 \cdot \gamma_j$ for $(j = 1, \ldots, Q)$. Since

ISBN: 978-3-95450-211-0 doi:10.18429/JACoW-SRF2019-THP102

Table 1: Mean Values $\overline{x}_j$ and Standard Deviations γ_j of Random Input Variables

Name	$\overline{x}_j$	γ_j
p_1 (gap)	0.54 [mm]	0.054 [mm]
p_2 (rrods)	13.40 [mm]	1.34 [mm]
p_3 (rloop)	4.73 [mm]	0.4725 [mm]
p_4 (dloop)	5.20 [mm]	0.52 [mm]
p_5 (wloop)	39.76 [mm]	3.976 [mm]
p_6 (rcoil)	22.41 [mm]	2.241 [mm]
p_7 (angleBentRight)	0.0 [deg]	0.33 [deg]
p_8 (angleBentLeft)	0.0 [deg]	0.33 [deg]
p_9 (angleTiltSpleOx)	0.0 [deg]	0.33 [deg]
p_{10} (angleTiltSpleOy)	0.0 [deg]	0.33 [deg]

the Stroud-3 formula is applied to determine the polynomial coefficients, it requires $K = 20$ deterministic simulations of the finite elements model. For this purpose, CST STUDIO SUITE® has been used. For some input variables that largely break the symmetry of the structure (e.g. large values of p_7 and p_8), the operating mode divided into two modes of the same type. The energy of each mode was more concentrated around one of the pair of rods. In such cases where two modes with a field pattern similar to the operating mode existed, the one with higher value of f_2 was considered as the operating mode. The results for the global sensitivity analysis conducted for the operating frequencies of the QPR are shown in Figs. 2,3 and 4. Finally, a detailed analysis of the QPR design versus uncertain geometrical parameters is summarized in Tables 2, 3 and 4. Additionally, we computed approximations of the PDF for the chosen random functionals (11a), (11c) and (11f) for the Gaussian input variables $\boldsymbol{\xi}$ using the response surface models (5), see Figs. 5–7.

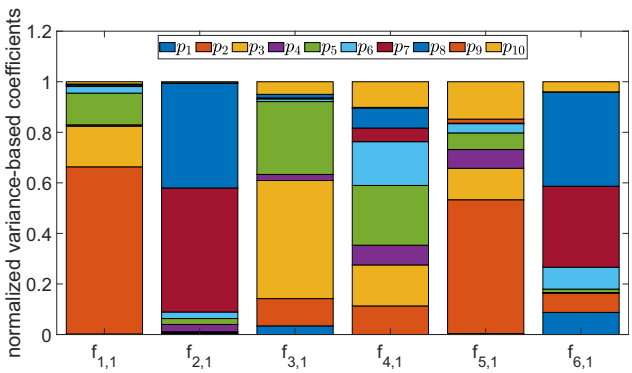

Figure 2: Result of the global sensitivity analysis for the first mode.

CONCLUSION

In our study, we have successfully conducted the UQ analysis considering three operating frequencies in order to investigate the impact of uncertain geometrical parameters related to manufacturing tolerances/imperfections onto the design of the QPR. Specifically, a variance-based sensitivity analysis seems to be a very promising and useful tool. It allows for determining the most influential input parameters, which are predominately responsible for the variation of ob-

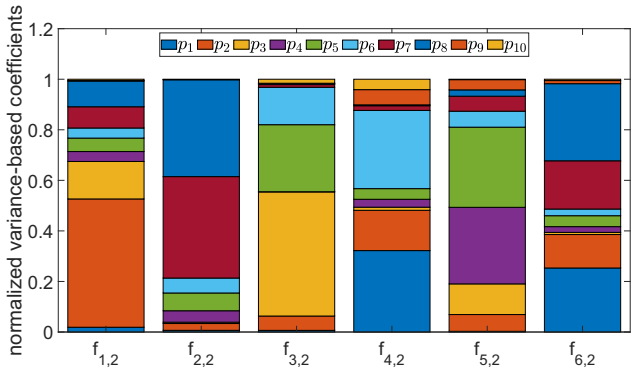

Figure 3: Result of the global sensitivity analysis for the second mode.

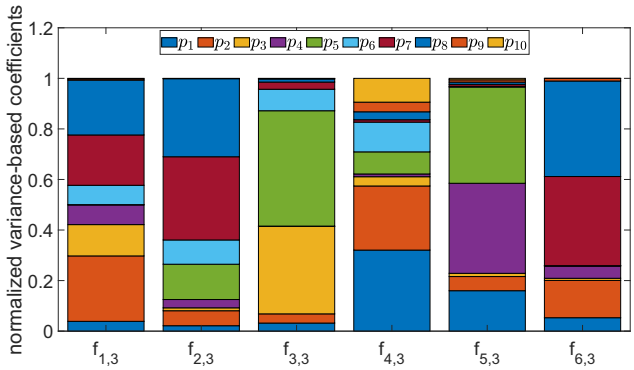

Figure 4: Result of the global sensitivity analysis for the third mode.

Table 2: Mean Values and Standard Deviations of Objective Functions for the First Mode

Symbol	$\mathbb{E}\left[f_j(\boldsymbol{p})\right]$	$\sqrt{\mathrm{Var}\left[f_j(\boldsymbol{p})\right]}$
f_1	0.422136 [GHz]	8.5744 [MHz]
f_2	6.2040e+07 $[A^2/J]$	2.5793e+07 $[A^2/J]$
f_3	0.1297 [1/1]	0.0194 [1/1]
f_4	0.8454[1/1]	0.0401 [1/1]
f_5	8.9747 [mT/(MV/m)]	1.6767 [mT/(MV/m)]
f_6	2.1080e+06 [1/1]	1.5469e+06 [1/1]

Table 3: Mean Values and Standard Deviations of Objective Functions for the Second Mode

Symbol	$\mathbb{E}\left[f_j(\boldsymbol{p})\right]$	$\sqrt{\mathrm{Var}\left[f_j(\boldsymbol{p})\right]}$
f_1	0.8543 [GHz]	11.139 [MHz]
f_2	5.3379e+07 $[A^2/J]$	2.4072e+07 $[A^2/J]$
f_3	0.1236 [1/1]	0.0205 [1/1]
f_4	0.8232 [1/1]	0.0709 [1/1]
f_5	5.4384 [mT/(MV/m)]	0.7539 [mT/(MV/m)]
f_6	1.0125e+06 [1/1]	8.9645e+05 [1/1]

ISBN: 978-3-95450-211-0 doi:10.18429/JACoW-SRF2019-THP102

Table 4: Mean Values and Standard Deviations of Objective Functions for the Third Mode

Symbol	$\mathbb{E}\left[f_j(\boldsymbol{p})\right]$	$\sqrt{\mathrm{Var}\left[f_j(\boldsymbol{p})\right]}$
f_1	1.3003 [GHz]	11.145 [MHz]
f_2	5.1766e+07 $[A^2/J]$	2.16e+07 $[A^2/J]$
f_3	0.1148 [1/1]	0.0142 [1/1]
f_4	0.8404 [1/1]	0.0544 [1/1]
f_5	3.9581 [mT/(MV/m)]	0.5316 [mT/(MV/m)]
f_6	2.3394e+05[1/1]	1.8041e+05 [1/1]

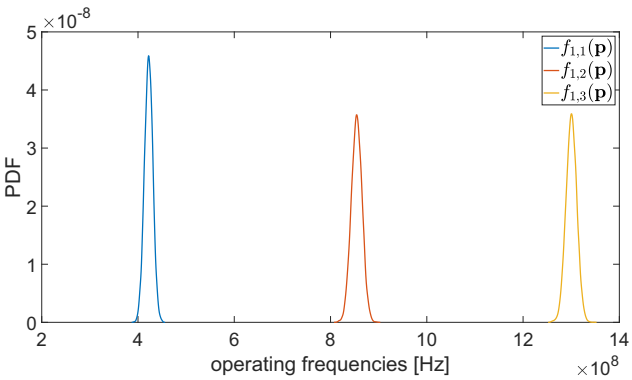

Figure 5: PDF of functional (11a), i.e. of the three operating frequencies.

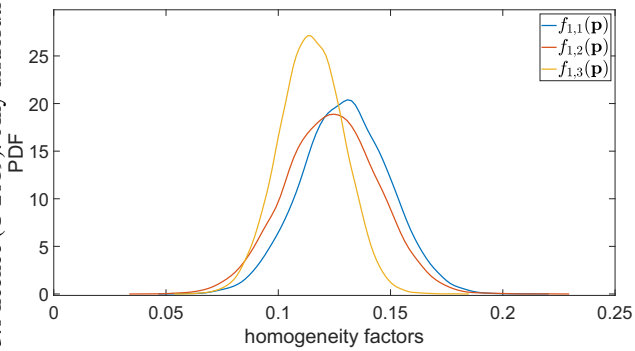

Figure 6: PDF of functional (11c), i.e. of the homogeneity factor for the three operating frequencies.

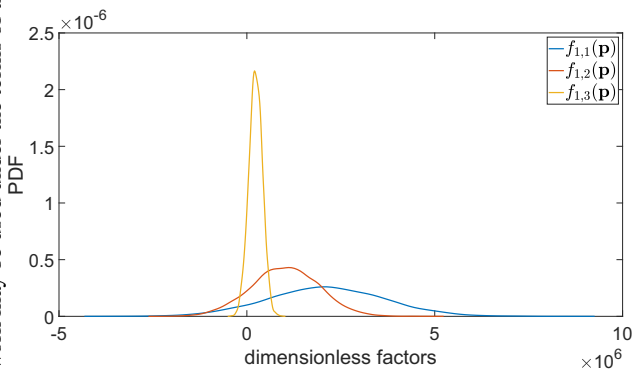

Figure 7: PDF of functional (11f), i.e. of the dimensionless factor to study measurement bias.

jective functions. Results of this decomposition are shown in Figs. 2, 3 and 4. This knowledge is essential during the optimization of the QPR under uncertainties. Though we considered the preliminary robustly optimized structure of the QPR [8], the influence of the bending angle seems to be crucial for the functioning of the QPR. The small value of f_6 for the third mode (in comparison with the other two operating modes) is an indication that the field of this mode penetrates deeper into the coaxial gap around the calorimetry chamber. This allows for explaining the problems with the measurement bias of the surface resistance at the third mode. In order to further investigate this phenomenon and the influence of the bending of the rods during operation of the cavity, the electromagnetic-stress coupled problem needs to be formulated and solved. This will be considered as a future research direction.

REFERENCES

[1] E. Mahner, S. Calatroni, E. Chiaveri, E. Häbel, and J. M. Tessier, "A new instrument to measure the surface resistance of superconducting samples at 400 MHz", *Review of Scientific Instruments*, vol. 74, no. 7, pp. 3390–3394, 2003.

[2] R. Kleindienst, "Radio Frequency Characterization of Superconductors for Particle Accelerators", Ph.D. dissertation, Universität Siegen, Germany, 2017.

[3] R. Kleindienst, O. Kugeler, and J. Knobloch, "Development of an Optimized Quadrupole Resonator at HZB", in *Proc. SRF'13*, Paris, France, Sep. 2013, paper TUP074, pp. 614–616.

[4] S. Aull, S. Doebert, T. Junginger, and J. Knobloch, "High Resolution Surface Resistance Studies", in *Proc. SRF'13*, Paris, France, Sep. 2013, paper WEIOC01, pp. 785–788.

[5] D. Xiu, "Efficient Collocational Approach for Parametric Uncertainty Analysis", *Commun. in Comput. Phys.*, vol. 2, no. 2, pp. 293–309, 2007.

[6] P. Putek, "Nonlinear magnetoquasistatic interface problem in a PM machine with stochastic PDE constraints," *Engineering Optimization*, pp. 1–24, Mar. 2019.

[7] S. Keckert, T. Junginger, O. Kugeler, J. Knobloch, "The Challenge to Measure n Surface Resistance on SRF Samples", in *Proc. IPAC'18*, Vancouver, Canada, Apr.-May 2018, pp. 2812–2815. doi:10.18429/JACoW-IPAC2018-WEPML049

[8] P. Putek, S. Gorgi Zadeh, M. Wenskat, O. Kugeler and U. van Rienen, "Shape optimization of quadrupole resonator for the RF characterization of superconductors", in *Proc. of COMPUMAG 2019*, Paris, France. (to appear)

[9] D. Xiu, "Numerical Methods for Stochastic Computations: A Spectral Method Approach", Princeton University Press, 2010.

[10] B. Sudret, "Global sensitivity analysis using polynomial chaos expansions", *Reliability Engineering & System Safety*, vol. 93, no. 7, pp. 964–979, 2008.

[11] P. Putek, E. J. W. ter Maten, M. Günther, and J. K. Sykulski, "Variance-based robust optimization of a Permanent Magnet synchronous machine", *IEEE Trans. on Magn.*, vol. 54, no. 3, Art no. 8102504, 2018.